Journal of
Materials Chemistry A

Materials for energy and sustainability

Accepted Manuscript

This article can be cited before page numbers have been issued, to do this please use: J. Guillen Campos, M. Park, Y. Wu, S. Sandlass, E. M. Novikov, S. J. Bailey, M. J. Gordon, T. Timofeeva and J. Read de Alaniz, *J. Mater. Chem. A*, 2025, DOI: 10.1039/D5TA01043H.

ROYAL SOCIETY OF CHEMISTRY

rsc.li/materials-a

View Article Online
DOI: 10.1039/D5TA01043H

ARTICLE

Synthesis of Photoresponsive Liquid Crystal Elastomers: A General Chemical Approach

Received 00th January 20xx,
Accepted 00th January 20xx

DOI: 10.1039/x0xx00000x

Jesus Guillen Campos,[a†] Minwook Park,[a†] Yuhang Wu,[a] Sara Sandlass,[b] Egor M. Novikov,[c] Sophia, J. Bailey,[a] Michael Gordon,[b] Tatiana V. Timofeeva,[b] and Javier Read de Alaniz,*[a]

Liquid crystal elastomers represent a versatile class of polymer materials with potential applications in soft robotics, adhesives, and smart materials. The integration of photoresponsive molecules into LCEs enables spatiotemporal control, wavelength-selective actuation and remote operations, expanding their application space. However, the incorporation of sensitive photoresponsive molecules is often hindered by the chemical methods and processing conditions required for the LCE fabrication. In this work, we introduce a general strategy for covalent incorporation of photoresponsive moieties into LCEs through Diels–Alder chemistry, utilizing late-stage functionalization. This approach facilitates the retention of material alignment and thermomechanical properties, while enabling the functionalization of thick, aligned polysiloxane elastomers. A wide range of photoresponsive molecules, including azobenzenes, spiropyrans, cyanine dyes, and donor-acceptor Stenhouse adducts, were successfully integrated, demonstrating this method's versatility. Furthermore, we leverage the reversible nature of Diels–Alder conjugation to achieve on-demand editing and exchange of photoresponsive moieties within a single LCE, allowing for dynamic tuning of material properties. This platform offers a scalable and efficient route for developing multifunctional LCEs, providing new opportunities for advanced stimuli-responsive materials and broadening the scope of applications across various fields.

Introduction

Liquid crystal elastomers (LCEs) are a class of programmable materials capable of delivering reversible optical, mechanical, and molecular responses by harnessing the liquid crystal phase transition and entropic elasticity of their polymeric networks.[1] To enable motion – a critical feature for advancing artificial muscles,[2,3] soft robotics[4–8] and "life-like" actuators[9–12]– the fabrication of a liquid crystal monodomain (or single-crystal orientation) with thermodynamically stable, aligned mesogens is typically necessary. In addition to preparing aligned LCEs, careful consideration must also be given to the type of stimuli-responsive species integrated into the LCE material,[13] as this influences the choice of stimuli (e.g., light, heat, pH, magnetic fields), alignment strategy, film thickness, and the suitability of the LCE for specific applications. From a technological perspective, the stimuli used to trigger actuation should be tunable, capable of generating fast, high-power actuation, safe for human contact, readily accessible, and compatible with stimuli-responsive species that are easy to integrate into the synthetic strategies for preparing LCEs. Achieving this balance presents significant technical challenges, including identifying viable stimuli-responsive species and optimizing the fabrication of the corresponding aligned LCEs.

In 1991, Finkelmann and Küpfer pioneered a two-stage hydrosilylation method, achieving the first "nematic liquid single crystal elastomers" capable of free-standing actuation.[14] This two-stage approach exploited the kinetic difference in crosslinking, providing the opportunity to first establish the internal uniaxial alignment field through mechanical stretching on a lightly cured gel (first-stage), and then the slower second-stage, providing a sufficient processing window to permanently fix that alignment. To achieve more complex patterns of LC alignment, other techniques have been developed to keep the mesogens oriented during synthesis, including surface alignment,[15] 3D printing,[16] and magnetic fields.[9] These advancements necessitated the development of new chemistry to prepare the network and permanently secure the more complex LC alignment. The commercial availability of diacrylate reactive monomers, such as RM257 and RM82, along with the introduction of a two-stage Michael addition (thiol-Michael or aza-Michael) and photopolymerization reaction,[17,18] helped shift the field away from the classical Finkelmann method. These methods typically rely on an initial oligomerization or chain extension of the difunctional acrylates via a Michael conjugate addition reaction, followed by an independent photo-polymerization to secure the aligned monodomain.[19] These techniques are also favored because they allow easy tuning of desired material properties, such as glass transition

[a] Department of Chemistry and Biochemistry, University of California, Santa Barbara. Santa Barbara, California 93106, United States
[b] Department of Chemical Engineering, University of California, Santa Barbara. Santa Barbara, California 93106, United States
[c] Department of Chemistry, New Mexico Highlands University, Las Vegas, New Mexico, 87701, United States
† Authors contributed equally.

Supplementary Information available: [details of any supplementary information available should be included here]. See DOI: 10.1039/x0xx00000x

View Article Online
DOI: 10.1039/D5TA01043H

ARTICLE

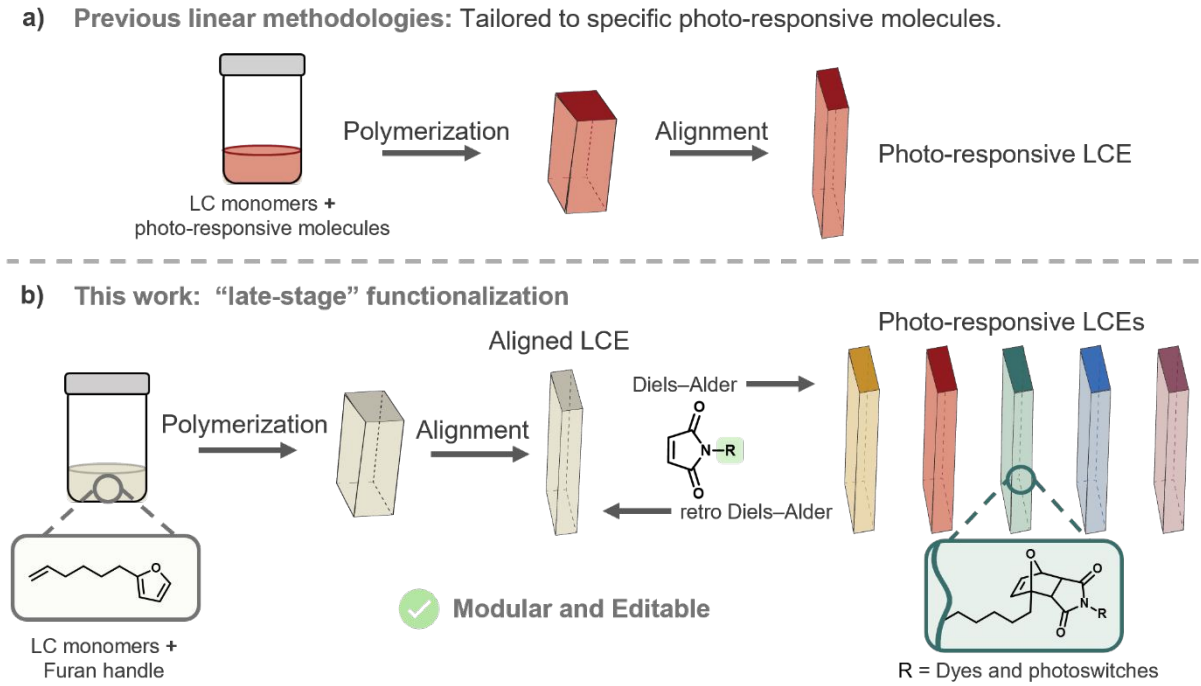

Figure 1. a) Previous linear methodologies for the introduction of photoresponsive molecules in LCEs. b) New general late-stage functionalization strategy to enable modular and editable introduction of photoresponsive molecules in LCEs through Diels–Alder (DA) and retro Diels–Alder reactions (rDA).

temperature (T_g), nematic-to-isotropic transition temperature (T_{ni}), and storage modulus (G').[19] Although these approaches are widely used and have exceptional spatio-temporal control of the second-stage photopolymerization, the use of photopolymerization imposes limits on the thickness due to light penetration depth and generality of the stimuli-responsive species used in LCE fabrication.

Nevertheless, in recent years, the power of this approach has been showcased by the introduction of state-of-the-art azobenzenes,[20–22] diarylethenes,[23,24] hydrazones,[25] gold nanoparticles,[26,27] and molecular machines.[28] These light-controlled LCEs allow for remote operation with exceptional spatial and temporal precision, often achieving cutting-edge functionality. However, exploring new photoresponsive molecules (PRMs) or optimizing light-controlled LCE properties for specific applications remains challenging due to the chemical compatibility requirements of PRMs with fabrication techniques (i.e., nucleophilic addition and radical reactions), as well as the difficulty in predicting the optimal PRM for a given specific application. Progress is further hindered by the requirement to incorporate photoresponsive molecules into LCEs during the initial oligomerization or lightly-crosslinked gel phase, necessitating full optimization of LCE fabrication conditions to explore different photoresponsive molecules (**Figure 1a**). To enable a general platform to explore a wide variety of photoresponsive molecules in LCEs, it would be advantageous to incorporate the photoresponsive molecules after the aligned LCE properties have been established. By separating the LCE fabrication from the incorporation of the photo-responsive molecule, each step can be tuned and optimized independently. This should prove useful for fundamental reaction-structure-property relationships studies and to enable the use of a vast library of state-of-the-art photoresponsive molecules.

Recently, we introduced a new late-stage functionalization strategy to successfully introduce donor-acceptor Stenhouse adducts (DASAs) into LCEs for the first time using Finkelmann's two-stage hydrosilylation method.[29] Notably, this new method facilitates the incorporation of DASA, which has traditionally been incompatible with LCE synthesis, and enabled the fabrication of thick, aligned films while preserving their thermomechanical properties. To generalize this late-stage functionalization approach for a variety of photoresponsive molecules, we envisioned the incorporation of furan as a universal "click handle" to incorporate photoresponsive molecules into LCEs using a Diels–Alder (DA) cycloaddition (**Figure 1b**). We were drawn to this method because furan is compatible with the two-step platinum-catalyzed

View Article Online
DOI: 10.1039/D5TA01043H

hydrosilylation process[30] and the DA cycloadditions between furan and maleimide can occur at room temperature, is radical free and can occur without a catalyst. Moreover, the furan–maleimide DA reaction is reversible at relatively modest temperature (~110 °C), introducing a novel feature for light-responsive LCEs: the ability to "edit" their light-responsive properties and reuse the LCE scaffold.

In this report, we demonstrate the synthesis and alignment of furan functionalized LCEs using hydrosilylation of olefinic liquid crystalline monomers and mechanical alignment to produce polysiloxane elastomers with thickness up to 400 µm. A variety of maleimide functionalized PRMs were clicked into the LCEs *via* late-stage functionalization (**Figure 1b**). The late-stage functionalization is conducive with the aligned polysiloxane LCEs, preserving the thermomechanical properties and material alignment. To showcase the generality of this method, a library of light-responsive LCEs were prepared including photoswitches and photothermal agents. By leveraging the retro-Diels–Alder cycloaddition, the photoresponsive molecule was exchanged, enabling the photoresponsive properties to be modified without re-fabricating the material. We believe this new method can serve as a general platform for the functionalization, characterization, and comparison of PRMs in LCEs.[31]

Results and discussion

Characterization and effect of furan loading in polysiloxane-based LCEs

The polysiloxane liquid crystal elastomers examined in this study are comprised of traditional olefinic mesogens[14] and a new furan click handle. To investigate the stability of the furan handle in the hydrosilylation reaction, ^{1}H NMR spectroscopy experiments were performed without the crosslinker. Treatment of 2-(hex-5-en-1-yl)-furan (0.5 eq., 0.7 mol, 106 mg) with PHMS (1.0 eq, 1.4 mol, 85 mg) and platinum catalyst (10 µL of a 1 wt.% solution in dichloromethane) in 1.5 mL of toluene at 70 °C (**Figure 2a)**. ^{1}H NMR (in deuterated chloroform) spectrum shows a slight shift of the distal hydrogens of the furan aromatic ring due to the change in electronic environment as the furan group is incorporated into the polymer backbone (blue shaded peaks), **Figure 2b**. The incorporation of the olefinic furan is further observed by the protons in the α-carbon position of the furan (**Figure S1**) where the triplet slowly shifts to a broad band peak at upper fields. Despite changes in peak multiplicity, the integrations of the hydrogen signals remained constant. This suggests that the furan aromatic ring was preserved during the hydrosilylation reaction. Finally, the disappearance of the terminal vinyl hydrogens in the 5.0-5.9 ppm region (purple shaded peaks) and the appearance of new peaks in the 0.5-0.6 ppm region (red shaded peaks) indicate successful attachment to the siloxane backbone **Figure 2c**. Full ^{1}H-NMR spectrum is reported in Supplementary Information, **Figure S1**.

With NMR studies confirming the incorporation of the furan handle into hydrosilylation reaction, we next investigated the aligned furan-functionalized LCE film properties. We initially

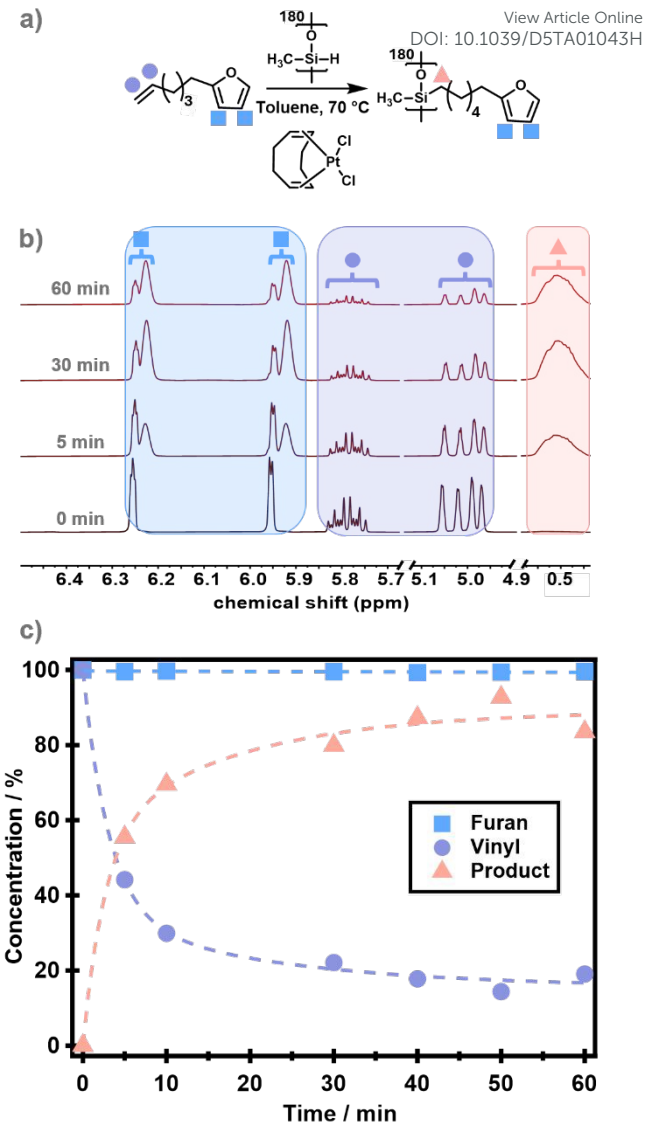

Figure 2. a) Reaction of 2-(hex-5-en-1-yl)-furan (furan handle) with PHMS (DP = 180) in toluene using a platinum catalyst at 70 °C for one hour. b) ^{1}H NMR traces of the hydrosilylation reaction of the furan handle with PHMS from 0 to 60 minutes where consumption of the terminal vinyl group is monitored while the integration of furan aromatic hydrogens remains constant. c) Plot of the conversion of the hydrosilylation reaction.

targeted 1 wt.% furan loading. A mixture of high molecular weight polymethylhydrosiloxane (PHMS), 4-methoxyphenyl 4-(but-3-en-1-yloxy)benzoate (liquid crystal mesogen), dichloro(1,5-cyclooctadiene)platinum(II) (catalyst) and 2-(hex-5-en-1-yl)-furan (click handle) were dissolved in toluene (**Figure 3a**). This mixture was placed in a custom-built spinning Teflon mold and was heated to 70 °C for 1 h and spun at 8000 prm.[14] Afterwards, the reaction was stopped by placing the centrifuge in dry ice for five minutes or until it reached room temperature. The resulting organo-gel was extracted from the walls of the centrifuge and the films were mechanically aligned by placing in a custom stretcher for two days before characterization and post-functionalization experiments (**Figure 3b**). Experimental details can be found in the supplementary information, **Table S1**.

View Article Online
DOI: 10.1039/D5TA01043H

Two-dimensional wide angle X-ray scattering (2DWAXS) revealed that alignment was not disrupted by the incorporation of furan functional group into the LCE at 1 wt.%, **Figure S2**. Two distinct regions of high intensity in the equatorial plane were observed, indicating an anisotropic molecular packing of the rod-like structure of the liquid crystals. An order parameter of S ≈ 0.7 was calculated, which is comparable with the degrees of order reported originally by Finkelmann.[14] The polarized optical microscopy (POM) images qualitatively support the X-ray scattering data, showing strong birefringence at 45 º tilted angle in the LCEs (**Figure S3**).

As expected for LCEs,[32] the nematic-to-isotropic temperature decreased with the reduction in the liquid crystal mesogen mass content and the corresponding increase in non-mesogen furan functional groups, as evident by DSC studies (**Figure S4-S5**). Specifically, the furan concentration was varied from 0 wt.% to 10 wt.% (~22 mol%). At 0 wt.% furan addition, a T_{ni} of approximately 80 °C was observed, which decreased to 30 ºC at 10 wt.% furan content. Increasing furan content also led to an observed decrease in the glass transition temperature from ≈ 5 °C down to -10 °C, presumably due to the disruption of molecular packing by alkyl chains. Finally, to assess the change in molecular packing of the aligned films, 2D WAXS was conducted as shown in **Figure S6-S7**. We observed a small change in the order parameter from S ≈ 0.7 at 0 wt.% to S ≈ 0.56 at 5 wt.% furan content. In contrast, at 10 wt.% furan content the order parameter decreased to approximately S ≈ 0.3. Due to the more significant drop in order parameter at 10 wt%, the percent furan incorporation was kept below 1 wt. % for subsequent studies.

Synthesis via late-stage functionalization of photoresponsive molecules in polysiloxane-based LCE

After synthesis of the aligned furan functionalized LCE, the late-stage Diels–Alder cycloaddition was evaluated. Prior to the introduction of the photoresponsive molecules into the LCEs, the platinum catalyst was removed to avoid potential side reactions with the PRMs by swelling the films in toluene for one hour and then in dichloromethane for another three hours exchanging the solvent every hour. Of note, the order of swelling was selected to avoid mechanical tearing of the films that occurs when the films were directly introduced in dichloromethane. The Diels–Alder late-stage functionalization was conducted by immersing the films into a solution containing the maleimide-functionalized PRMs in dichloromethane (DCM) at room temperature (5 mL, 0.02 M) (**Table S2**). To ensure efficient functionalization, the films were reacted for three days and then washed three times with DCM to remove excess maleimide-PRM. Subsequently, the solvent was exchanged from DCM to toluene (by submerging the film in toluene for one hour) and the resulting gels were dried for three days under reduced pressure. 2D WAXS measurements showed that drying time under reduced pressure exhibited a strong impact on the measured order parameter, with residual trapped toluene in the network disrupting molecular packing of the liquid crystals, see Supplementary Information and **Figure S8** for details.

The incorporation of a range of PRMs with different chemical reactivity and switching properties was utilized to demonstrate the generality of this method (**Figure 2**). To benchmark the method, we first incorporated traditional azobenzene photoswitch and disperse red azobenzene dye into the network. These photoresponsive molecules are widely used due to their robustness and compatibility with most LCE polymerization techniques and, as expected, they integrated without complication. Next, we selected spiropyrans for incorporation into the LCE because they are a privileged class of photochromic material with a rich photochemical history.[33] Despite their significant potential in LCEs, they remain largely underexplored due to synthetic challenges associated with LCE fabrication.[34] Spiropyrans are known to chelate with metals which can compromise incorporation via platinum catalysed hydrosilylation reaction. Moreover, the open merocyanine form are susceptible to nucleophilic addition, restricting use of Michael addition methodologies for LCE preparation.[35–37] To our delight, using the new Diels–Alder based post-functionalization approach spiropyran can be readily incorporated. Finally, to underscore the versatility and broad applicability of this method, we selected cyanine-5 dye (blue dye) and a DASA-based photoswitch, both of which are highly prone to degradation in the presence of free radicals, nucleophiles, and metal catalysts. Moreover, the high molar absorptivity of these dyes limits light penetration, which typically restricts fabrication to thin films. As shown in **Figure 3c**, the successful incorporation of a range of photoresponsive molecules opens new avenues for the development of advanced photoresponsive materials. Detailed spectral properties, synthetic procedure of the small molecule PRMs and additional characterization of each LCE film can be found in the Supporting Information (**Figure S9-S23**).

Characterization of the late-stage functionalized polysiloxane-based LCEs

To access the material properties after the late-stage functionalization with the corresponding PRM, the glass transition temperature, nematic-to-isotropic temperature (**Figure S24-S26**) and order parameter (**Figure S27-S51**) were determined with networks prepared from 1, 5, and 10 wt% incorporation (**Figure S52-S71**). **Figure 4a** illustrates the decrease in glass transition temperature (T_g) observed over this range. A similar effect was observed with the attachment of the furan handle alone. Notably, for azobenzene and the disperse red dye, T_g remained stable between 1 and 5 wt.% loading. In contrast, for spiropyran, DASA and the blue dye, T_g exhibited a linear decrease with increasing concentration. Despite this trend, the overall change in T_g was minimal – around 10 °C after introduction of 10 wt.% furan handle – rendering the effect negligible for most practical applications. **Figure 4b** shows that

View Article Online
DOI: 10.1039/D5TA01043H

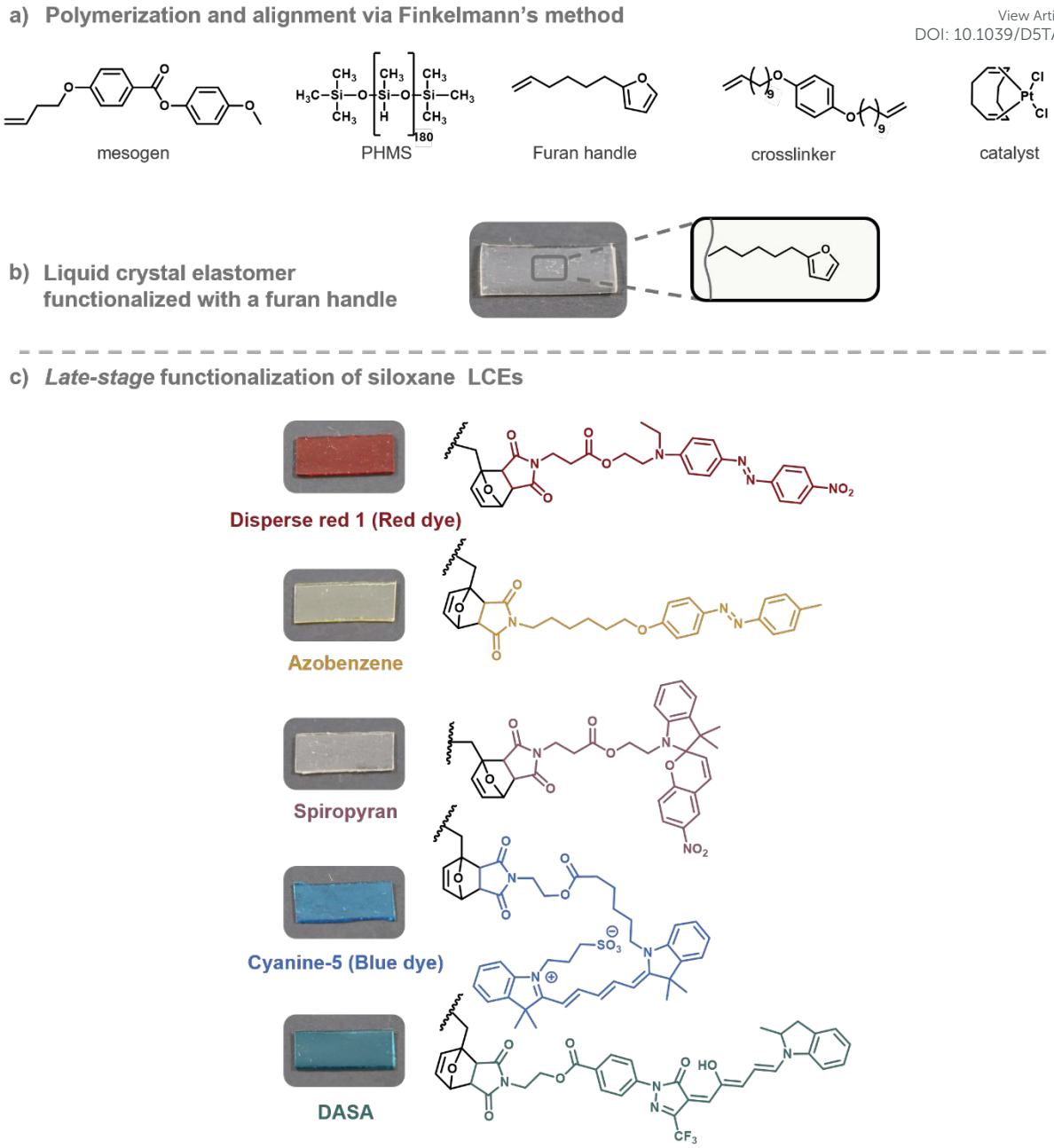

Figure 3. a) Monomers used for the fabrication of furan-functionalized liquid crystal elastomers. b) Furan-functionalized LCE c) Late-stage functionalized LCEs with PRMs.

the nematic-to-isotropic transition temperature shifts more significantly, decreasing from approximately 80 °C in the absence of PRMs to around 30 °C at 10 wt.% furan handle loading. Interestingly, the nematic-to-isotropic transition decreased by 20 ºC when the furan handle loading was increased from 0 to 5 wt.% but the change in T_{ni} was not observed after functionalization with azobenzene or disperse red dye. This suggests that these two molecules act as mesogen, restoring order and enhancing the thermodynamic stability to the network. The trend in T_{ni} aligns with results from 2DWAXD order parameter studies (**Figure 4c**). A key distinction between the order parameter and T_{ni} behavior is that while the order parameter remains relatively stable up to 5 wt%, it rapidly drops at 10 wt% to the lower limit for aligned liquid crystals (S ≈ 0.3) across all PRMs. Due to differences in chemical structure and molecular weight, the overall mass gain of LCEs after late-stage functionalization varies depending on the PRMs used. In an effort to account for these structure property relationship differences, the data was replotted as a function of total mass (Supplementary Information, **Figures S72-S74**) but no major difference was observed.

An unexpected observation is that the PRMs tend to "self-align" in the nematic direction. This self-alignment is evident by the linear dichroism observed in the synthesized LCEs. To study this linear dichroism, linearly polarized solid-state UV-Visible spectroscopy was performed, as shown in **Figure 4d** and **Figure**

View Article Online
DOI: 10.1039/D5TA01043H

ARTICLE

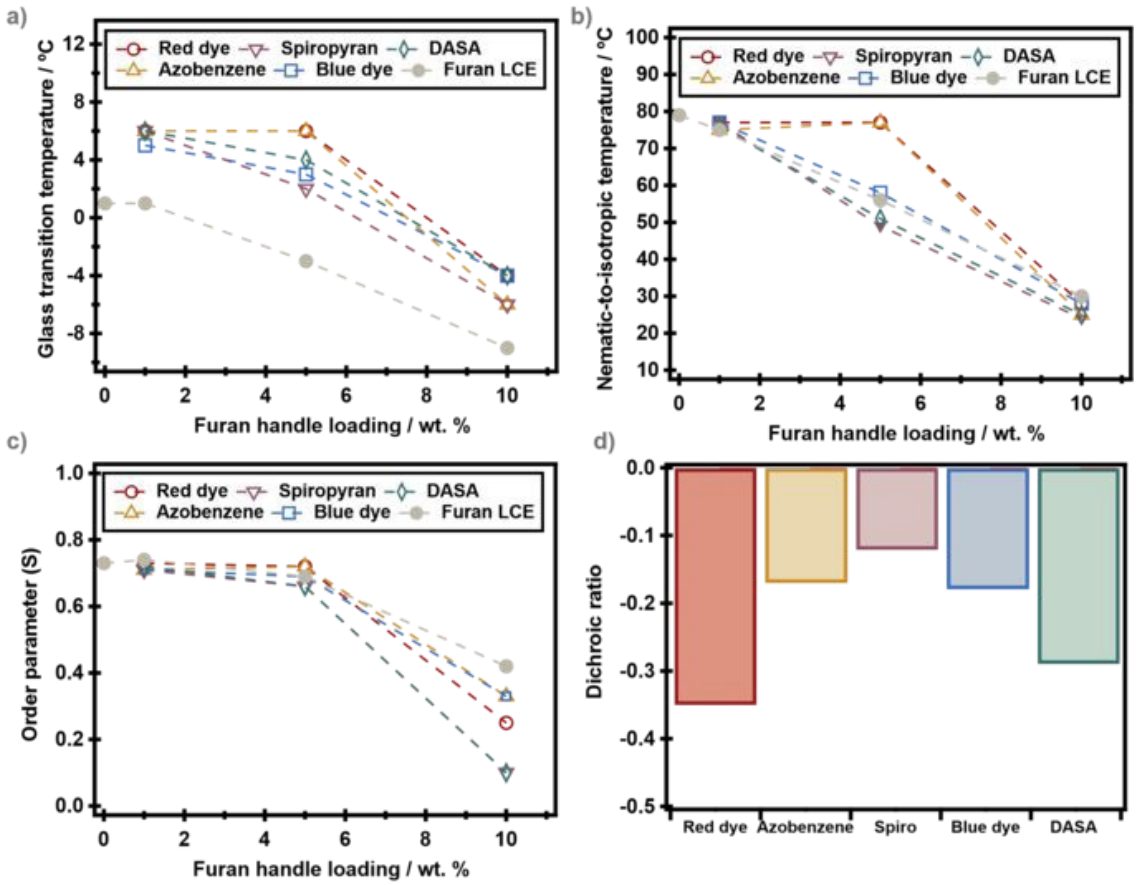

Figure 4. a) Plot of the effect of the PRM loading in the LCE in the glass transition temperature as recorded by DSC at a heating rate of 10 °C per minute. b) Effect of the loading of the PRM in the nematic to isotropic temperature obtained by DSC. c) Order parameter as a function of the introduced PRM determined by 2D WAXD. d) Linear dichroism of the introduced PRMs in the siloxane LCEs determined by polarized UV-Vis spectroscopy.

S75-S79. These results indicate that spiropyran, the bulkiest molecule, has the lowest linear dichroism, indicating a reduced degree of alignment in the nematic direction. In contrast, DASA and the disperse red dye show the highest linear dichroism amongst the five molecules. This is attributed to their elongated structures, which allow them to intercalate between mesogens, enhancing alignment. Note, the effect of the transition dipole moment may also play a role in the structural characteristics of the dye and their orientational behavior.[38]Taken together, these results demonstrate the versatility and generality of this new universal platform.

Photo-responsive properties of the polysiloxane-based LCEs

For the photomechanical actuation studies, we fabricated LCEs 2 cm in length (0.5 cm wide and 400 µm thick) and with 1 wt% PRM loading. The contraction parallel to the director in response to different irradiation conditions was used to visualize the mechanical response, shown in **Figure 5.** Such contractions occur primarily due to the photothermal effect, where the PRM absorbs the photons, transfer the photon energy to heat, and subsequently trigger the contraction of the LCE. Photothermal-driven contraction was selected for its ease of visualizing deformation, enabling straightforward comparison of various photoresponsive agents, including both photoswitches and dyes. We note that at this stage, no meaningful comparisons between photoresponsive agents and magnitude of contraction should be concluded. This will require more detailed studies and optimization of photomechanical process for each PRM (e.g., light intensity, absorption wavelength, molar absorptivity, irradiation times, film thickness, thermal gradients, strain rates, PRM loading and extra). For example, UV-light exposure of 1 W•cm^{-2} brings only a small contraction after ~40 seconds of irradiation to the azobenzene functionalized film (**Figure 5a**). This is explained by

View Article Online
DOI: 10.1039/D5TA01043H

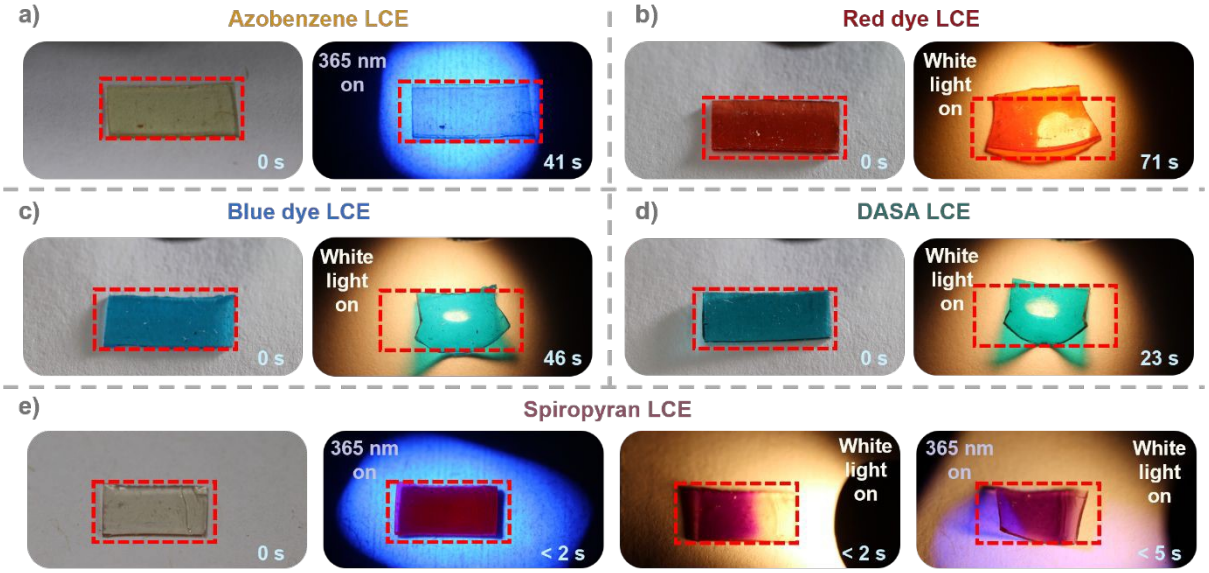

Figure 5. a) Azobenzene LCE before and during UV light irradiation. b) Disperse red dye LCE before and during white light irradiation. c) Blue dye LCE before and during white light irradiation. d) DASA LCE before and during white light irradiation. e) Spiropyran LCE before light irradiation and during UV light irradiation (left two boxes). Spiropyran LCE exposed to white light irradiation and exposed to both UV and white light irradiation (right two boxes).

the UV-Vis data (**Table S3**) and molar absorptivity. The overlapping absorbance bands of azobenzene and the LCE mesogens, along with the low molar absorptivity of azobenzene, contribute to the reduced photothermal efficiency under these conditions. In contrast, the LCEs that contain the disperse red dye (**Figure 5b**), blue dye (**Figure 5c**) and DASA (**Figure 5d**) with high molar absorptivity in the visible region contracted to a significantly higher extent, and faster with white light irradiation (300 mW•cm^{-2}).

Spiropyran-based LCE offered unique multi-responsive properties. As shown in **Figure 5e**, UV-light irradiation alone induces neither photothermal nor photochemical actuation. However, when UV and visible light are applied simultaneously the photothermal deformation is clearly observed. This demonstrates an AND-gate photoactuation mechanism that can be described as follows: (1) If no light is applied, the spiropyran remains in its transparent form, generating no photothermal heat or action; (2) when only UV light is applied, the spiropyran converts to its merocyanine form, changing the film's color and enhancing visible light photothermal absorption. However, without visible light, no photothermal heating or actuation occurs; (3) if only visible light is used, the spiropyran remains transparent and no photothermal heating or actuation is observed. Even if visible light is applied to the merocynanine form, the rapid reformation of transparent spiropyran prevents significant photothermal heating; (4) by applying both light inputs simultaneously, the AND-gate activates, leading to photothermal deformation. The simultaneous application established an equilibrium between spiropyran and merocyanine forms, allowing continuous photon absorption and generating sufficient heat to drive film contraction. This type of behavior was first demonstrated with diarylethene-driven LCN by Zeng and Priimagi,[23] however, to our knowledge has not been demonstrated with other classes of photochromes. This mechanism highlights the dynamic control and responsiveness of spiropyran-based systems for photothermal applications and highlights the potential of incorporating new photochromic molecules into LCEs to enable enhanced performance. Videos for each PRM contraction can be found in the supplemental information **Video S1-S5**.

Editing of LCEs using the Diels–Alder based platform

We anticipated that the retro-DA (rDA) reaction of the furan–maleimide Diels–Alder chemistry and ability to post-functionalize the aligned LCE without disrupting the fabricated LCE properties may offer the ability to "edit" the nature of the photochrome within the LCE matrices. Although others have demonstrated the use of dynamic bonds to reprocess LCE films,[24,39,40] the LCE films made here are not re-polymerized or re-aligned, instead the photothermal agent is un-clicked and a new photothermal agent is clicked into the LCE. To demonstrate this concept, a disperse red dye LCE containing 1 wt% of furan loading, **Figure 6a**, was synthesized as detailed in the Supplementary Information. The disperse red LCE was then submerged in toluene at room temperature and subsequently the solution was heated to 110 °C. At this temperature the rDA reaction is facilitated and the disperse red can be visually observed in the toluene solution. The solution was exchanged three times over the course of three hours (one hour each) to remove the disperse red dye. At this stage the film was visually transparent, and the toluene solution was exchanged for a 0.02 M DASA solution in DCM. The film was allowed to soak overnight to enable the re-functionalization of the LCE with DASA (**Figure 6b**). Solid state broad band UV-Vis and 2D WAXD experiments were performed on the original disperse red films

View Article Online
DOI: 10.1039/D5TA01043H

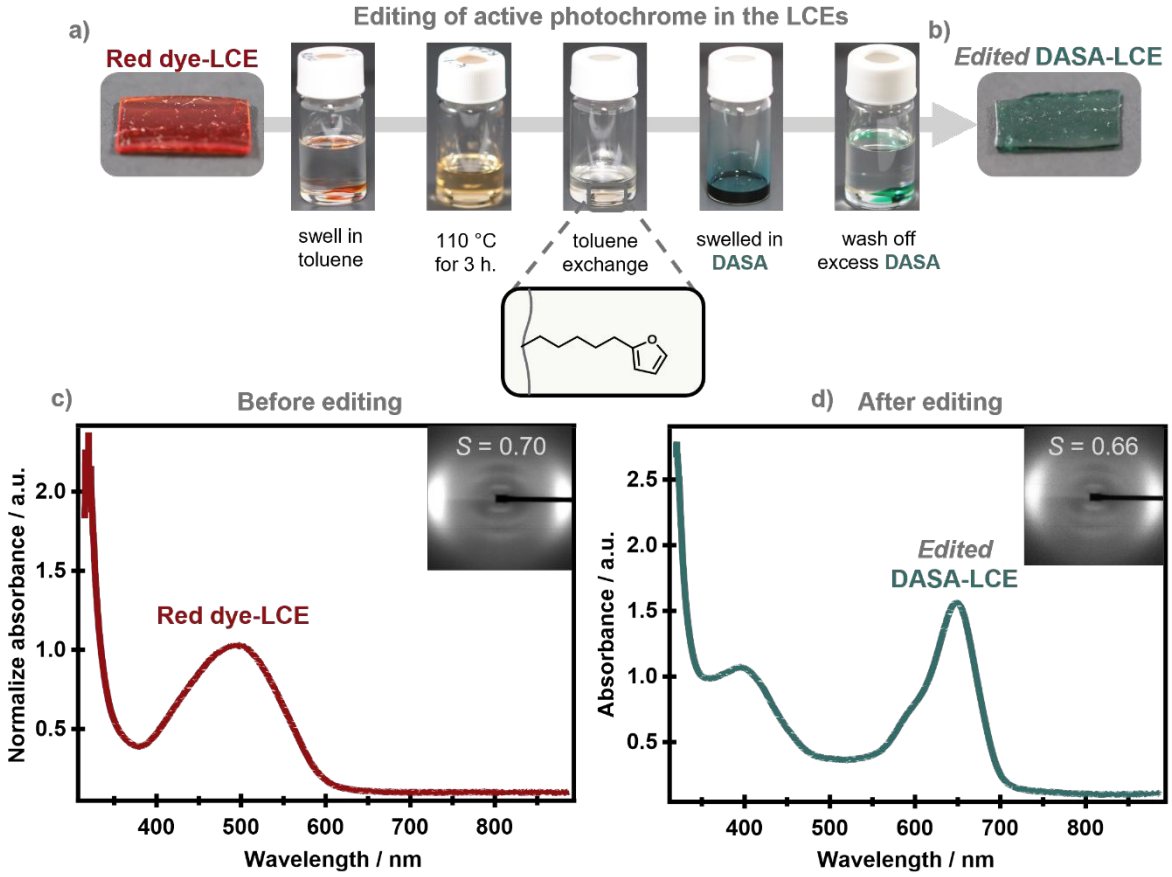

Figure 6. a) Disperse red dye LCE before editing. b) Edited DASA LCE after undergoing rDA to cleave the disperse red dye and subsequent swelling of DASA. c) Solid-state absorbance trace of the disperse red dye LCE and 2D WAXD before editing. d) Solid-state absorbance trace of the edited DASA LCE and 2D WAXD showing retention of the order parameter.

(**Figure 6c**), and after DASA incorporation (**Figure 6d**) to determine the spectral properties and the degree of alignment. Spectroscopically, the maximum absorption peak of disperse red dye is around 490 nm and after thermally driven retro-DA, the absorbance in that region is negligible compared to the new maximum absorbance corresponding to the DASA peak at 650 nm. The order parameter, after this chemical exchange of the photoresponsive molecule showed a small decrease going from S ≈ 0.7 to S ≈ 0.66. Additional examples of editing the nature of the photoresponsive agent without re-processing the entire material can be found in **Figure S85-S86**. Future studies will focus on quantifying the efficiency of this process and highlighting the dynamic control enabled by incorporating multiple orthogonal responsive photoresponsive agents.

Conclusions

In this work, we demonstrated a general strategy for the covalent incorporation of photoresponsive molecules into liquid crystal elastomers (LCEs) using Diels–Alder chemistry for late-stage functionalization. This approach preserves the thermomechanical properties and alignment of the polysiloxane elastomers, enabling the creation of thick, well-aligned LCE films. The versatility of the method was showcased by incorporating a diverse library of photoresponsive molecules, including azobenzene, spiropyran, cyanine dye and donor-acceptor Stenhouse adducts (DASAs), each offering unique actuation responses to different wavelengths of light. By leveraging the reversible nature of the Diels–Alder reaction, we further demonstrated the ability to edit and exchange photoresponsive moieties within the LCE matrix, allowing on-demand tuning of material properties. However, understanding the efficiencies of the DA and rDA reactions, as well as their dynamic control and temperature dependence, particularly near the T_{ni} (80 °C) is critical. Future work will focus on elucidating these structure-property relationships. This late-stage functionalization approach not only simplifies the incorporation of sensitive PRMs but also expands the design space for stimuli-responsive LCEs, unlocking new possibilities in applications such as soft robotics, adhesives, and protective materials.

Author contributions

CRediT: Jesus Guillen Campos methodology (lead), data curation (equal), writing-original draft (lead), Minwook Park data curation (lead), methodology (equal), writing-review & editing (equal), Yuhang Wu methodology (equal), Sara Sandlass data curation (equal), writing-review & editing (equal), Egor M. Novikov methodology (equal), Sophia J. Bailey methodology (equal), Tatiana V. Timofeeva supervision (lead), writing-review & editing (equal), Michael Gordon supervision (lead), writing-review & editing (equal), Javier Read de Alaniz formal analysis (equal), writing-review & editing (lead), supervision (lead).

Conflicts of interest

There are no conflicts to declare.

Data availability

The data supporting this article have been included as part of the Supporting Information. The data analysis scripts of this article are available at Dryad at DOI: .

Acknowledgements

The research was funded by the National Science Foundation (CHE-2204077). We are grateful for support of EMN, TVT and JRdA from the National Science Foundation PREM award DMR-2122108 and BioPACIFIC Materials Innovation Platform award DRM-1933487. The NMR instruments were supported by the National Science Foundation under award No. MRI-1920299.

Notes and references

1 H. Finkelmann, H.-J. Kock, G. Rehage, *Makromol. Chem., Rapid Commun.,* 1981, **2**, 317.
2 M. Lahikainen, H. Zeng, A. Priimagi, *Nat. Commun.,* 2018, **9**, 4148.
3 H. Zeng, O. M. Wani, P. Wasylczyk, R. Kaczmarek, A. Priimagi, *Adv. Mat.,* 2017, **29**, 1701814.
4 T. Zhao, W. Fang, Y. Fan, Z. Hu, H. Wu, X. Q. Feng, J. an Lv, *Adv. Mater. Technol.,* 2022, **7**, 2101660.
5 Z. Hu, Y. Li, T. Zhao, J. an Lv, *Appl. Mater. Today.,* 2022, **27**, 2352.
6 M. Wang, X. B. Hu, B. Zuo, S. Huang, X. M. Chen, H. Yang, *Chem. Commun.,* 2020, **56**, 7597.
7 H. Shahsavan, A. Aghakhani, H. Zeng, Y. Guo, Z. S. Davidson, A. Priimagi, M. Sitti, *Proc. Natl. Acad. Sci. USA.,* 2020, **117**, 5125.
8 Y. Yu, T. Ikeda, *Angew. Chem. Int. Ed.,* 2006, **45**, 5416.
9 S. Li, M. M. Lerch, J. T. Waters, B. Deng, R. S. Martens, Y. Yao, D. Y. Kim, K. Bertoldi, A. Grinthal, A. C. Balazs, J. Aizenberg, *Nature*., 2022, **605**, 76–83.
10 H. Shahsavan, S. M. Salili, A. Jákli, B. Zhao, *Adv. Mat.,* 2017, **29**, 1604021.
11 Z. Liu, H. K. Bisoyi, Y. Huang, M. Wang, H. Yang, Q. Li, *Angew. Chem. Int. Ed.,* 2022, **61**, 2115755.
12 H. Zeng, H. Zhang, O. Ikkala, A. Priimagi, *Matter*, 2020, **2**, 194.
13 T. Ikeda, J. I. Mamiya, Y. Yu, *Angew. Chem. Int. Ed.,* 2007, **46**, 506.
14 J. Kiipfec, H. Finkelmann. *Makromol. Chem. Rapid Commun.,* 1991, **726**, 717.
15 H. H. Yoon, D. Y. Kim, K. U. Jeong, S. K. Ahn, *Macromolecules*, 2018, **51**, 1141.
16 A. Kotikian, R. L. Truby, J. W. Boley, T. J. White, J. A. Lewis, *Adv, Mat.,* 2018, **30**, 1706164.
17 C. M. Yakacki, M. Saed, D. P. Nair, T. Gong, S. M. Reed, C. N. Bowman, *RSC Adv.,* 2015, **5**, 18997.
18 Y. Li, T. Liu, V. Ambrogi, O. Rios, M. Xia, W. He, Z. Yang, ACS Appl Mater Interfaces, 2022, **14**, 14842–14858.
19 K. M. Herbert, H. E. Fowler, J. M. McCracken, K. R. Schlafmann, J. A. Koch, T. J. White, *Nat. Rev. Mater.,* 2022, **7**, 23.
20 K. Kumar, C. Knie, D. Bléger, M. A. Peletier, H. Friedrich, S. Hecht, D. J. Broer, M. G. Debije, A. P. H. J. Schenning, *Nat. Commun.,* 2016, **7**, 11975.
21 D. Ditter, L. B. Braun, R. Zentel, *Macromol. Chem. Phys.,* 2020, **221**, 1900265.
22 S. Iamsaard, E. Anger, S. J. Aßhoff, A. Depauw, S. P. Fletcher, N. Katsonis, *Angew. Chem. Int. Ed.,* 2016, **55**, 9908.
23 M. Lahikainen, K. Kuntze, H. Zeng, S. Helantera, S. Hecht, A. Priimagi, *ACS Appl. Mater. Interfaces,* 2020, **12**, 47939–47947.
24 T. S. Hebner, M. Podgórski, S. Mavila, T. J. White, C. N. Bowman, *Angew. Chem. Int. Ed.,* 2022, **61**, 2116522.
25 A. Ryabchun, Q. Li, F. Lancia, I. Aprahamian, N. Katsonis, *J. Am. Chem. Soc.,* 2019, **141**, 1196–1200.
26 A. S. Kuenstler, Y. Chen, P. Bui, H. Kim, A. DeSimone, L. Jin, R. C. Hayward, *Adv. Mat.,* 2020, **32**, 2000609.
27 M. M. Wójcik, J. Wróbel, Z. Z. Jan´czuk, J. Jan´czuk, J. Mieczkowski, E. Górecka, J. Choi, M. Ho, D. Pociecha. *Chem. Eur. J.,* 2017, **23**, 8912.
28 J. Hou, G. Long, W. Zhao, G. Zhou, D. Liu, D. J. Broer, B. L. Feringa, J. Chen, *J. Am. Chem. Soc.,* 2022, **144**, 6851–6860.
29 J. Guillen Campos, C. Tobin, S. Sandlass, M. Park, Y. Wu, M. Gordon, J. Read de Alaniz, *Adv. Mat.,* 2024, **36**, 2404932.
30 P. Azadi Namin, P. Booth, J. Treviño Silva, L. J. Voigt, P. M. Zelisko, *Macromolecules,* 2023, **56**, 2038.
31 I. Aprahamian, *ACS Cent. Sci.,* 2020, **6**, 347.
32 M. Barnes, S. Cetinkaya, A. Ajnsztajn, R. Verduzco, *Soft Matter,* 2022, **18**, 5074.
33 J. Keyvan Rad, Z. Balzade, A. R. Mahdavian. *J. Photoch. Photobio. C*., 2022, **51**, 100487.
34 D. Han, X. Wang, S. Liu, Y. Zhang, C. Li, Y. Gao, J. Zhang, *Adv. Mater. Technol*., 2023, **8**, 2300175.
35 H. Liang, K. Dai, Z. Li, K. Xiong, M. Yan, Y. Tan, *Dyes Pigm.,* 2021, **184**, 108805.
36 A. K. Chibisov, H. Gorner, *Chemical Physics,* 1998, **237**, 425.
37 T. J. Feuerstein, R. Müller, C. Barner-Kowollik, P. W. Roesky, *Inorg. Chem.,* 2019, **58**, 15479.
38 D. H. Song, J. P. Kim, *Dyes Pigm*., 2009, **80**, 219.
39 Z. C. Jiang, Y. Y. Xiao, L. Yin, L. Han, Y. Zhao, *Angew. Chem. Int. Ed.,* 2020, **59**, 4925.
40 M. O. Saed, E. M. Terentjev, *Sci. Rep.,* 2020, **10**, 6609.